Phytochemistry 241 (2026) 114674

Contents lists available at ScienceDirect

Phytochemistry

journal homepage: www.elsevier.com/locate/phytochem

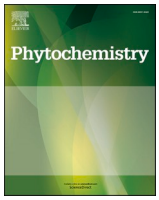

Undescribed antimicrobial labdane diterpenes from the flowers of *Euthamia graminifolia*

Márton Baglyas [a,b,*], Zoltán Bozsó [a], Ildikó Schwarczinger [a], Péter G. Ott [a], József Bakonyi [a], András Darcsi [c], Ágnes M. Móricz [a,**]

[a] Plant Protection Institute, HUN-REN Centre for Agricultural Research, Fehérvári út 132–144, 1116 Budapest, Hungary
[b] Doctoral School, Semmelweis University, Üllői út 26, 1085 Budapest, Hungary
[c] Pharmaceutical Chemistry and Technology Department, National Center for Public Health and Pharmacy, Szabolcs utca 33, 1135 Budapest, Hungary

ARTICLE INFO

Keywords:
Euthamia graminifolia (L.) Nutt.
Asteraceae
Grass-leaved goldenrod
Graminifolins A–E
Labdane diterpenes
TLC hyphenations
Antimicrobial activity

ABSTRACT

The demand for previously undescribed antimicrobial agents is increasing due to the emergence of resistant plant pathogens. One of the untapped sources of new biopesticides is the plant kingdom. A bioassay-guided process comprising TLC–*Bacillus subtilis* bioassay, TLC–MS, and preparative flash column chromatography enabled the isolation of five previously undescribed antimicrobial labdane diterpenes (graminifolins A–E, **1**–**5**) from the flower extract of grass-leaved goldenrod (*Euthamia graminifolia*, formerly known as *Solidago graminifolia*). Their structures were elucidated by NMR spectroscopy, supported by HRMS/MS, polarimetry, and UV, and ATR–FTIR spectroscopy. Graminifolins A–C (**1**–**3**) displayed low to moderate antibacterial and bactericidal activity against the Gram-positive plant pathogens *Curtobacterium flaccumfaciens* pv. *flaccumfaciens* and *Clavibacter michiganensis*, with MIC values between 67 and 533 μg/mL and MBC values ranging from 133 to 533 μg/mL. In contrast, graminifolin D+E (**4**+**5**) was active only against *C. michiganensis*. Among the isolated compounds, graminifolin A exhibited the strongest antibacterial effect and demonstrated weak antifungal activity against the crop pathogen *Bipolaris sorokiniana*. These findings underscore the potential of bioassay-guided fractionation in discovering previously undescribed bioactive compounds.

1. Introduction

The genus *Euthamia* (Nutt.) Cass. comprises various flowering plants within the family Asteraceae. Among the approximately 130 goldenrod species, including members of both the genera *Euthamia* and *Solidago* L., five are widely distributed across multiple European countries: the native *Solidago virgaurea* L. and the *Solidago canadensis* L., *Solidago gigantea* Ait., *Solidago rugosa* Mill., and *Euthamia graminifolia* (L.) Nutt (previously known as *Solidago graminifolia* (L.). Salisb.) with a North American origin (Szymura et al., 2019; Baglyas et al., 2023). *E. graminifolia*, commonly known as grass-leaved or flat-top goldenrod, was first cultivated for ornamental purposes in Europe probably around 1758 with naturalized populations first observed around the middle of the 19th century (Weber, 1998). It is a herbaceous perennial weed with allelopathic activity (Butcko and Jensen, 2002) that can negatively impact the yield of nearby crop species; therefore, its control is demanded in several agricultural systems such as blueberry fields (White et al., 2016). *E. graminifolia* is classified as an invasive species in Europe, as it spreads slowly via rhizomes, with almost no recruitment from seeds (Price et al., 2004). However, its occurrence remains sporadic and restricted to specific areas (Weber, 1998), including one Hungarian site (Schmotzer, 2008).

The decoctions of the roots and aboveground parts were historically used by native Americans to treat lung ailments and to alleviate fever and pain, respectively (Densmore, 2005). Previous studies demonstrated the bioactive potential of *E. graminifolia* extracts: the hydroalcoholic extract of aerial parts showed antioxidant and antibacterial activity against Gram-positive *Staphylococcus aureus*, and anti-yeast activity against *Candida albicans* and *Candida parapsilosis* (Toiu et al., 2019), whereas the ethanolic extract of leaves displayed insecticidal effects against *Spodoptera frugiperda* (Herrera-Mayorga et al., 2022).

Our previous studies revealed that goldenrod species (*S. canadensis*, *S. gigantea, S. rugosa, Solidago speciosa* Nutt., *S. virgaurea*, and *E. graminifolia*) are rich sources of bioactive specialized metabolites,

* Corresponding author. Plant Protection Institute, HUN-REN Centre for Agricultural Research, Fehérvári út 132–144, 1116 Budapest, Hungary.
** Corresponding author. Plant Protection Institute, HUN-REN Centre for Agricultural Research, Fehérvári út 132–144, 1116 Budapest, Hungary.
E-mail addresses: baglyas.marton@atk.hun-ren.hu (M. Baglyas), moricz.agnes@atk.hun-ren.hu (Á.M. Móricz).

https://doi.org/10.1016/j.phytochem.2025.114674
Received 1 April 2025; Received in revised form 6 September 2025; Accepted 7 September 2025
Available online 8 September 2025

including labdane, abietane, and clerodane diterpenes, polyacetylenes, and a benzyl benzoate derivative (Móricz et al., 2016, 2020, 2021; Krüzselyi et al., 2021; Baglyas et al., 2022, 2023). The occurrence of polyacetylenes in goldenrod species could be of chemotaxonomic significance. Roots of *E. graminifolia* contain polyacetylenes such as 2*Z*, 8*Z*-matricaria ester, *E*- and *Z*-dehydromatricaria esters, and 1,6*E*, 8*E*-hexadecatrien-10,12,14-triine (Lam et al., 1992; Krüzselyi et al., 2021). Various bioactive compounds have been reported from the aerial parts of *E. graminifolia*, including phenolic acids (*e.g.*, protocatechuic acid and *p*-coumaric acid) (Kalemba, 1992; Toiu et al., 2019), flavonoids (*e.g.*, quercetin and kaempferol) (Toiu et al., 2019; Thiem et al., 2001), caffeoylquinic acids (*e.g.*, chlorogenic acid) (Thiem et al., 2001), glycosylflavones (*e.g.*, schaftoside, isoschaftoside, hyperoside, and quercitrin) (Budzianowski, 1990; Toiu et al., 2019), and mono- and sesquiterpenoids (*e.g.*, sabinene, *β*-pinene, *p*-phellandrene, and germacrene D) (Kalemba et al., 1994; Kalemba and Thiem, 2004). Additionally, clerodane diterpene solidagoic acids B, C, and G have been described from the leaves (Herrera-Mayorga et al., 2022).

Polyacetylenes present in the roots of *E. graminifolia* displayed antibacterial (against *Bacillus subtilis*, *Aliivibrio fischeri*, and *Pseudomonas syringae* pv. *maculicola*), antifungal (against *Fusarium avenaceum* and *Bipolaris sorokiniana*), and enzyme inhibitory activity (*α*-glucosidase, *β*-glucosidase, *α*-amylase, acetylcholinesterase, and butyrylcholinesterase) (Móricz et al., 2016, 2020; Krüzselyi et al., 2021). Phenolic compounds are generally known as antioxidants capable of reducing the harmful effects of reactive oxygen species (Kruk et al., 2022). Abietane and clerodane diterpenes isolated from different *Solidago* species exhibited antibacterial and antifungal effect against various plant pathogens (Móricz et al., 2021; Krüzselyi et al., 2021; Baglyas et al., 2022, 2023).

In addition to their primary use in human healthcare, antibiotics are extensively employed in agriculture to prevent or cure bacterial infections and enhance crop productivity (Mann et al., 2021). However, their overuse and misuse have contributed to the constantly rising global antibiotic resistance crisis (Iwu et al., 2020). One potential solution to address this threat is the discovery of new antibacterial agents that can evade acquired resistance mechanisms.

As part of the ongoing search for previously undescribed antibiotics derived from invasive goldenrod plants, this study aimed at non-targeted, effect-directed screening, bioassay-guided isolation, and identification of antibacterial compounds from the methyl ethyl ketone extract of the grass-leaved goldenrod flowers. For this purpose, TLC hyphenations (UV, FLD, chemical derivatization, *B. subtilis* bioassay, and mass spectrometry (MS)), preparative flash column chromatography, flow injection analysis (FIA)–heated electrospray ionization (HESI)-tandem high-resolution MS (HRMS/MS), polarimetry, and UV, attenuated total reflectance Fourier-transform infrared (ATR–FTIR), and nuclear magnetic resonance (NMR) spectroscopy were utilized. The antibacterial and antifungal activities of the isolates were evaluated by *in vitro* microplate assays against the soil bacterium *B. subtilis*, the plant pathogens *Curtobacterium flaccumfaciens* pv. *flaccumfaciens*, *Clavibacter michiganensis*, *Pseudomonas syringae* pv. *tabaci*, and *Pseudomonas syringae* pv. *tomato*, as well as the fungal pathogens *Fusarium graminearum* and *Bipolaris sorokiniana*.

2. Results and discussion

2.1. Isolation and structure elucidation

The chemical and bio-profiles of *E. graminifolia* flower extract were studied by TLC separation combined with UV detection, vanillin–sulfuric acid derivatization, or *B. subtilis* bioassay detection (Fig. 1). Flash column chromatographic fractionation and purification steps were guided by TLC hyphenations and afforded five antibacterial isolates: **1**–**3** and **4**+**5** (Fig. 2).

The recorded one- and two-dimensional NMR (Figs. S5–S10 for **1**, S15–25 for **2**, S32–S37 for **3**, S44–S53 for **4**+**5**), HR-ESI-MS(/MS) (Figs. S11–S12 for **1**, S26–S29 for **2**, S38–S41 for **3**, S54–S55 for **4**+**5**), UV (Fig. S13 for **1**, S30 for **2**, S42 for **3**, S56 for **4**+**5**), and ATR-FTIR spectra (Fig. S14 for **1**, S31 for **2**, S43 for **3**, S57 for **4**+**5**) of compounds **1**–**5** can be found in the Supporting Information. The novelty of the structures of compounds **1**–**5** was confirmed by searching in CAS SciFinder® and Reaxys databases.

Graminifolin A (**1**) (Fig. 3) was obtained as a yellow oil with a specific optical rotation of $[\alpha]_D^{25}$ +8.9 (*c* 0.29, MeOH). The molecular formula of compound **1** was established as $C_{20}H_{32}O_3$ deduced from the ^{13}C NMR and negative-ion mode HESI-HRMS spectrum at *m/z* 319.2278 $[M-H]^-$ (calculated for $C_{20}H_{31}O_3^-$, *m/z* 319.2279 $[M-H]^-$, error: −0.2 ppm),

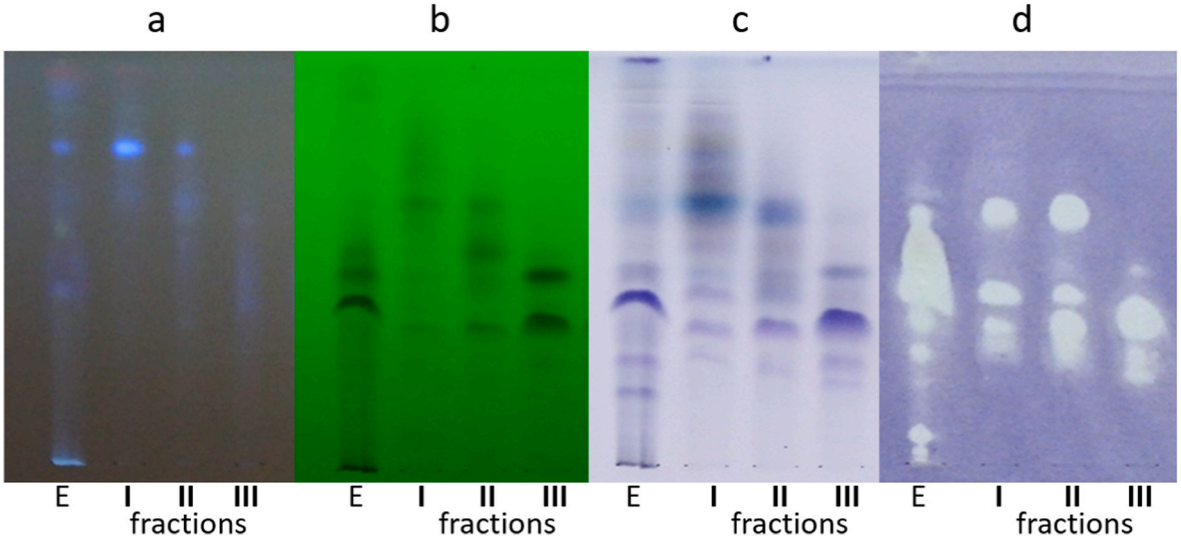

Fig. 1. TLC chromatograms (a–c) and bioautogram (d) of *Euthamia graminifolia* flower extract (E) and its fractions (**I**–**III**) obtained by preparative, normal-phase flash column chromatography, developed with isopropyl acetate – toluene – ethanol, 11:9:1 (*V/V*), documented at UV 366 nm (a), 254 nm (b), and white light illumination after vanillin–sulfuric acid derivatization (c), and effect-directed detection using *Bacillus subtilis* (d, bright zones against a purple background indicate antibacterial compounds).

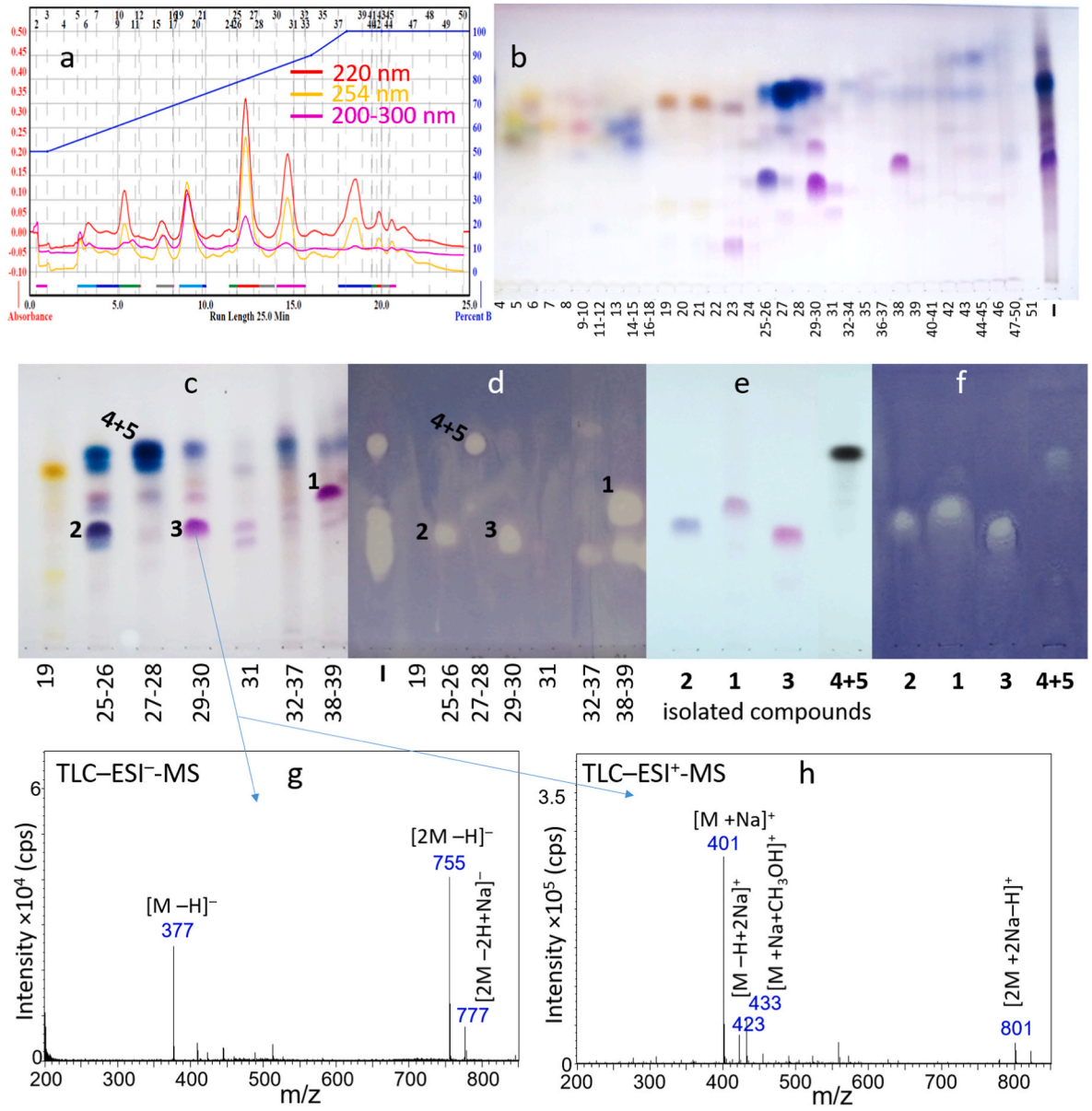

Fig. 2. TLC chromatograms of fractions (4–51) (b) and pooled fractions (19–39, respectively) (c) of *Euthamia graminifolia* flower extract obtained by the further purification of fraction **I** by preparative, reversed-phase flash column chromatography using water with 0.1% formic acid/methanol gradient (a) as well as isolated compounds (**1**–**5**) documented after derivatization with anisaldehyde reagent (b, c, e) and effect-directed detection using *Bacillus subtilis* (d, f, bright zones against a purple background indicate antibacterial compounds); TLC–ESI-MS spectra of the bioactive zone in fraction 29–30, corresponding to compound **3**, obtained in the negative (g) and positive (h) ionization modes via an elution-head based interface, and background subtraction are exemplarily shown along with the assignments.

indicating 5 double bond equivalents (DBEs). Its ^{1}H NMR spectrum (Table 1) exhibited proton resonances corresponding to five methyl groups at δ_H 2.14 (3H, d, J = 1.2 Hz, H$_3$-16), 1.72 (3H, br s, H$_3$-17), 0.96 (3H, s, H$_3$-19), 0.85 (3H, s, H$_3$-18), and 0.79 (3H, s, H$_3$-20), two vinylic hydrogens at δ_H 5.67 (1H, br s, H-14) and 5.42 (1H, br s, H-7), and an oxymethine group at δ_H 3.17 (1H, dd, J = 10.8, 5.0 Hz, H-3). Based on ^{13}C (Table 2), ^{1}H–^{13}C multiplicity-edited HSQC (edHSQC), and ^{1}H–^{13}C HMBC spectroscopic data, the twenty ^{13}C resonances were assigned to five methyl groups (δ_C 28.5, 22.3, 19.0, 15.7, 14.0), five aliphatic (δ_C 44.2, 38.6, 28.1, 26.6, 24.6) methylene groups, one oxygenated (δ_C 79.7), two olefinic (δ_C 123.6, 118.1), and two aliphatic (δ_C 55.5, 51.0) methine groups, and five non-hydrogenated carbons, including one carboxylic (δ_C 171.4), two olefinic (δ_C 159.8, 135.8), and two aliphatic (δ_C 39.7, 37.7) carbons. Thus, the structure of compound **1** exhibits two trisubstituted carbon-carbon double bonds and a carboxylic moiety implying a bicyclic molecule to satisfy the required number of DBEs. Besides, 30 hydrogen atoms can be accounted for and the remaining two exchangeable hydrogens were assigned to one hydroxy and one carboxylic group, which were supported by the characteristic broad IR absorption band at 3388 cm^{-1} (O–H stretch) and intense, sharp bands at 1692 cm^{-1} (α,β-unsaturated C=O stretch) and 1645 cm^{-1} (C=C stretch). These overall features implied that compound **1** has a labdane-type diterpene skeleton (Peters, 2010).

^{1}H–^{1}H COSY spectrum revealed three spin systems: H$_2$-1a/H$_2$-1b/H$_2$-2/H-3, H-5/H$_2$-6a/H$_2$-6b/H-7, and H-9/H$_2$-11a/H$_2$-11b/H$_2$-12a/H$_2$-12b (Fig. 4). ^{1}H–^{13}C HMBC correlations from H$_3$-18 to C-19 and from H$_3$-19 to C-18, and the fact that H$_3$-18 and H$_3$-19 shared all other correlations confirmed the presence of two geminal-related methyl groups. A hydroxy group was assigned to C-3, indicated by the downfield ^{1}H NMR chemical shift of H-3 (δ_H 3.17), and by long-range heteronuclear correlations from H-3 to C-4, from H$_3$-18 to C-3, and from H$_3$-19 to C-3. The resonance corresponding to the allylic methyl

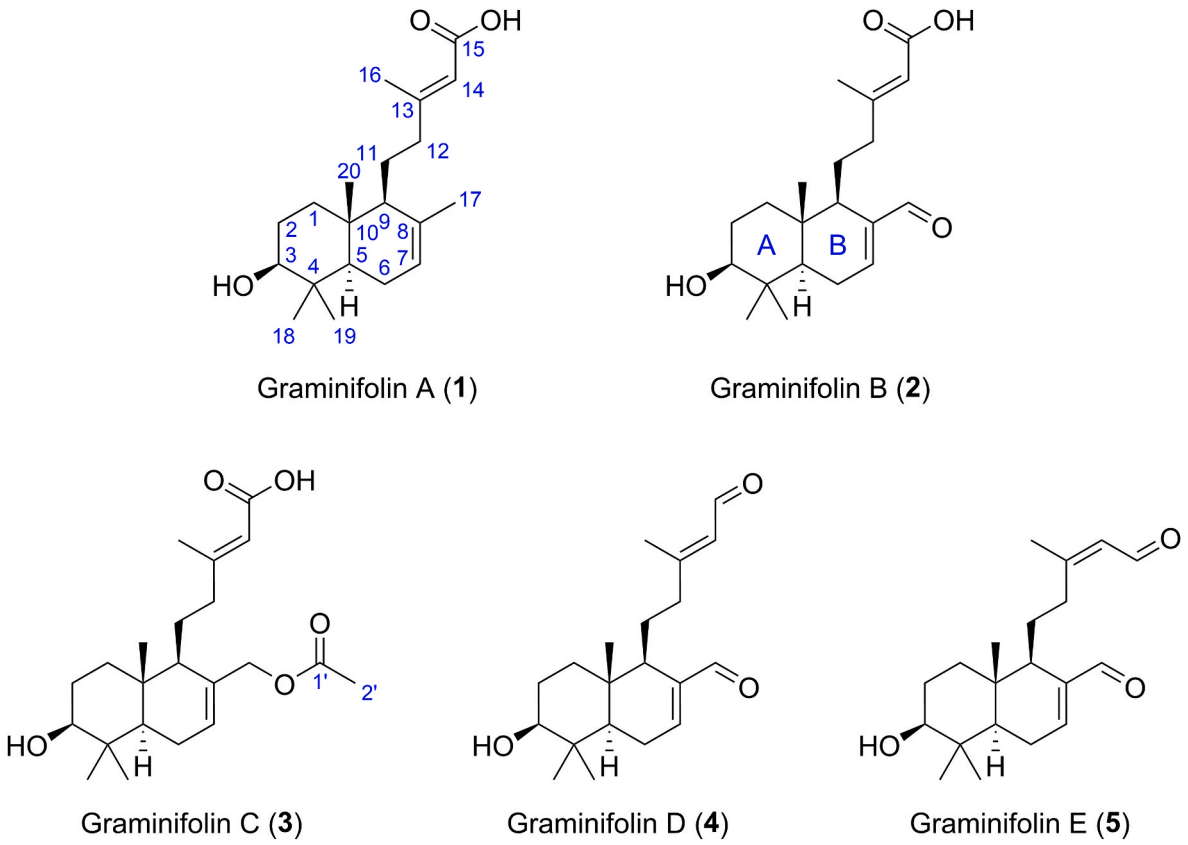

Fig. 3. The chemical structures of graminifolins A–E (**1**–**5**) with the atomic numbering (blue). (For interpretation of the references to color in this figure legend, the reader is referred to the Web version of this article.)

Table 1
^{1}H NMR (400 MHz) spectroscopic data of graminifolins A–E (**1**–**5**) (δ in ppm, J in Hz).

	Graminifolin A (1)[a]	Graminifolin B (2)[b]	Graminifolin C (3)[b]	Graminifolin D (4)[b]	Graminifolin E (5)[b]
Position	δ_H, mult. (J in Hz)	δ_H, mult. (J in Hz)	δ_H, mult. (J in Hz)	δ_H, mult. (J in Hz)	δ_H, mult. (J in Hz)
1a	1.90, dt (13.0, 3.4)	1.90, dt (13.4, 3.5)[d]	1.85, dt (13.0, 3.4)	1.92[c]	1.92[c]
1b	1.15, td (13.0, 4.9)	1.16, td (13.4, 4.0)[d]	1.10, td (13.0, 4.1)	1.20[c]	1.20[c]
2a	1.63[c]	1.66, m[d]	1.63[c]	1.63[c]	1.63[c]
2b		1.60, m[d]	1.59[c]		
3	3.17, dd (10.8, 5.0)	3.26, dd (11.4, 4.3)	3.24, dd (11.3, 4.4)	3.27[c]	3.27[c]
4	–	–	–	–	–
5	1.20[c]	1.21, dd (11.6, 5.2)[d]	1.22, dd (11.7, 5.1)	1.22[c]	1.22[c]
6a	1.99, m	2.34, m	2.07[c]	2.37[c]	2.37[c]
6b			1.99, m		
7	5.42, br s	6.82, dt (5.2, 2.6)	5.82, dt (5.3, 2.5)	6.84[c]	6.84[c]
8	–	–	–	–	–
9	1.65[c]	1.92, m	1.77, br s	1.94[c]	1.96[c]
10	–	–	–	–	–
11a	1.64[c]	1.58, m[d]	1.60[c]	1.61[c]	1.61[c]
11b	1.36, m		1.38, m		
12a	2.38, m	2.72, m	2.28, ddd (14.6, 10.8, 4.7)	2.80, m	3.05, td (12.0, 5.0)
12b	2.11, m	2.08, td (12.8, 5.6)	2.08[c]	2.14, m	2.63, td (12.0, 5.9)
13	–	–	–	–	–
14	5.67, br s	5.69, s	5.65, br s	5.89, br d (8.1)	5.84, br d (8.3)
15	–	–	–	9.98, d (8.1)	10.03, d (8.3)
16	2.14, d (1.2)	2.17, d (1.3)	2.13, d (1.3)	2.20, d (1.3)	2.02, d (1.3)
17a	1.72, br s	9.37, s	4.51, d (12.2)	9.39, s	9.40, s
17b			4.45, d (12.2)		
18	0.85, s	0.89, s	0.83, s	0.91, s	0.91, s
19	0.96, s	0.99, s	0.95, s	1.01, s	1.01, s
20	0.79, s	0.78, s	0.73, s	0.80, s	0.80, s
1’			–		
2’			2.04, s		

[a] Measured in CD_3OD.
[b] Measured in $CDCl_3$.
[c] Multiplicities and coupling constants not reported due to overlap of signals; chemical shifts determined from HSQC spectrum.
[d] Multiplicities and coupling constants determined from 1D selective TOCSY spectra (500 MHz).

Table 2
^{13}C NMR (101 MHz) spectroscopic data of graminifolins A–E (**1**–**5**) (δ in ppm).

	Graminifolin A (1)[a]	Graminifolin B (2)[b]	Graminifolin C (3)[b]	Graminifolin D (4)[b]	Graminifolin E (5)[b]
Position	δ_C, type	δ_C, type	δ_C, type	δ_C, type	δ_C, type
1	38.6, CH_2	36.8, CH_2	37.1, CH_2	36.9, CH_2	36.8, CH_2
2	28.1, CH_2	27.0, CH_2	27.1, CH_2	27.2, CH_2	27.2, CH_2
3	79.7, CH	78.8, CH	78.9, CH	78.8, CH	78.7, CH
4	39.7, C	38.6, C	38.7, C	38.7, C	38.7, C
5	51.0, CH	49.0, CH	49.0, CH	49.0, CH	48.9, CH
6	24.6, CH_2	25.1, CH_2	23.5, CH_2	25.2, CH_2	25.1, CH_2
7	123.6, CH	153.1, CH	130.0, CH	153.3, CH	153.5, CH
8	135.8, C	144.0, C	133.4, C	144.0, C	143.9, C
9	55.5, CH	50.1, CH	51.4, CH	50.2, CH	50.5, CH
10	37.7, C	36.6, C	36.6, C	36.7, C	36.6, C
11	26.6, CH_2	25.3, CH_2	24.7, CH_2	25.1, CH_2	27.0, CH_2
12	44.2, CH_2	43.1, CH_2	42.4, CH_2	42.7, CH_2	35.0, CH_2
13	159.8[c], C	163.8, C	162.3, C	165.4, C	165.7, C
14	118.1, CH	115.0, CH	115.7, CH	127.2, CH	128.4, CH
15	171.4[c], C	171.7, C	171.3, C	191.7, C	191.8, C
16	19.0, CH_3	19.2, CH_3	19.2, CH_3	17.7, CH_3	25.1, CH_3
17	22.3, CH_3	194.9, C	67.6, CH_2	194.8, C	194.8, C
18	15.7, CH_3	15.3, CH_3	15.2, CH_3	15.3, CH_3	15.3, CH_3
19	28.5, CH_3	27.9, CH_3	27.8, CH_3	28.0, CH_3	28.0, CH_3
20	14.0, CH_3	14.1, CH_3	13.7, CH_3	14.2, CH_3	14.1, CH_3
1′			171.0, C		
2′			21.2, CH_3		

[a] Measured in CD_3OD.
[b] Measured in $CDCl_3$.
[c] Chemical shifts determined from HMBC spectrum.

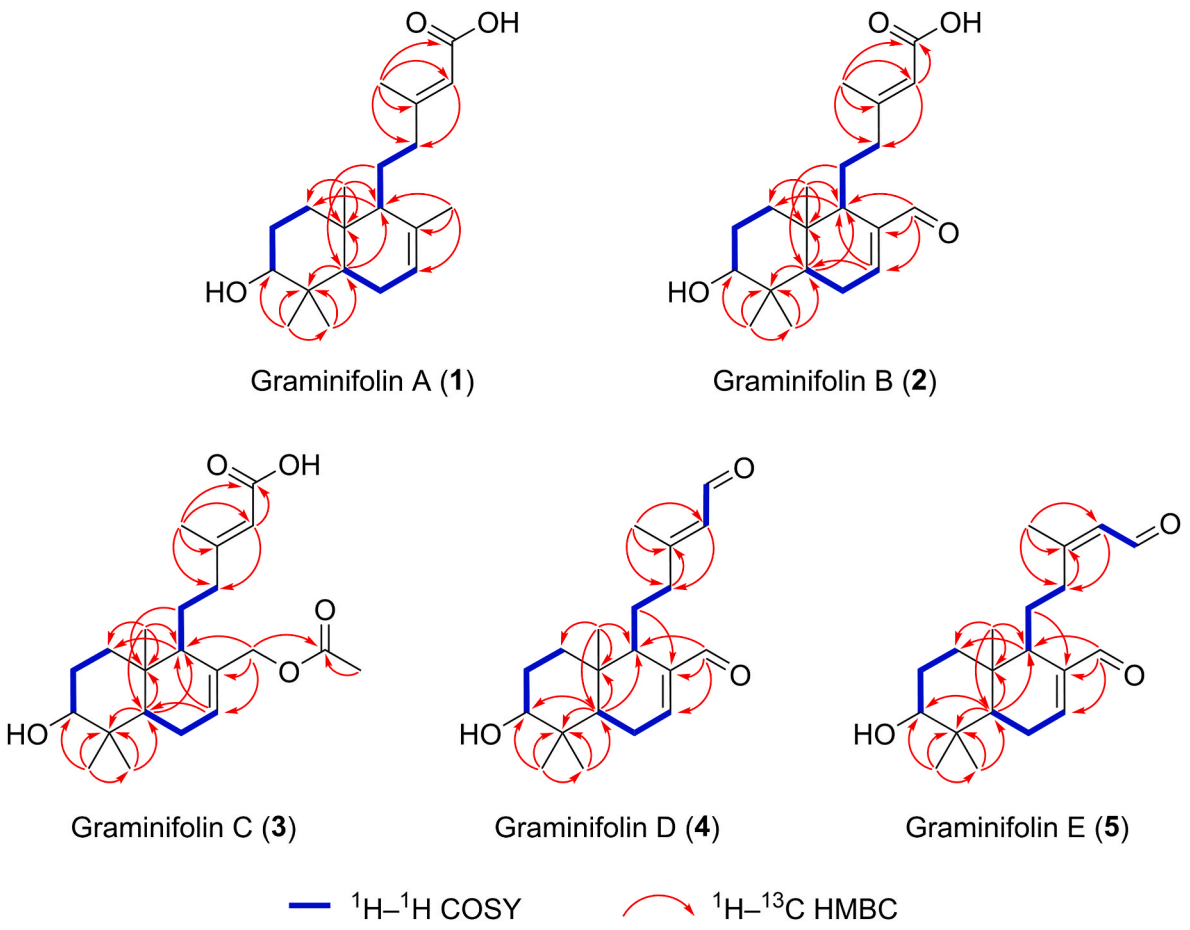

Fig. 4. Key ^{1}H–^{1}H COSY (blue) and ^{1}H–^{13}C HMBC (red) correlations of graminifolins A–E (**1**–**5**). (For interpretation of the references to color in this figure legend, the reader is referred to the Web version of this article.)

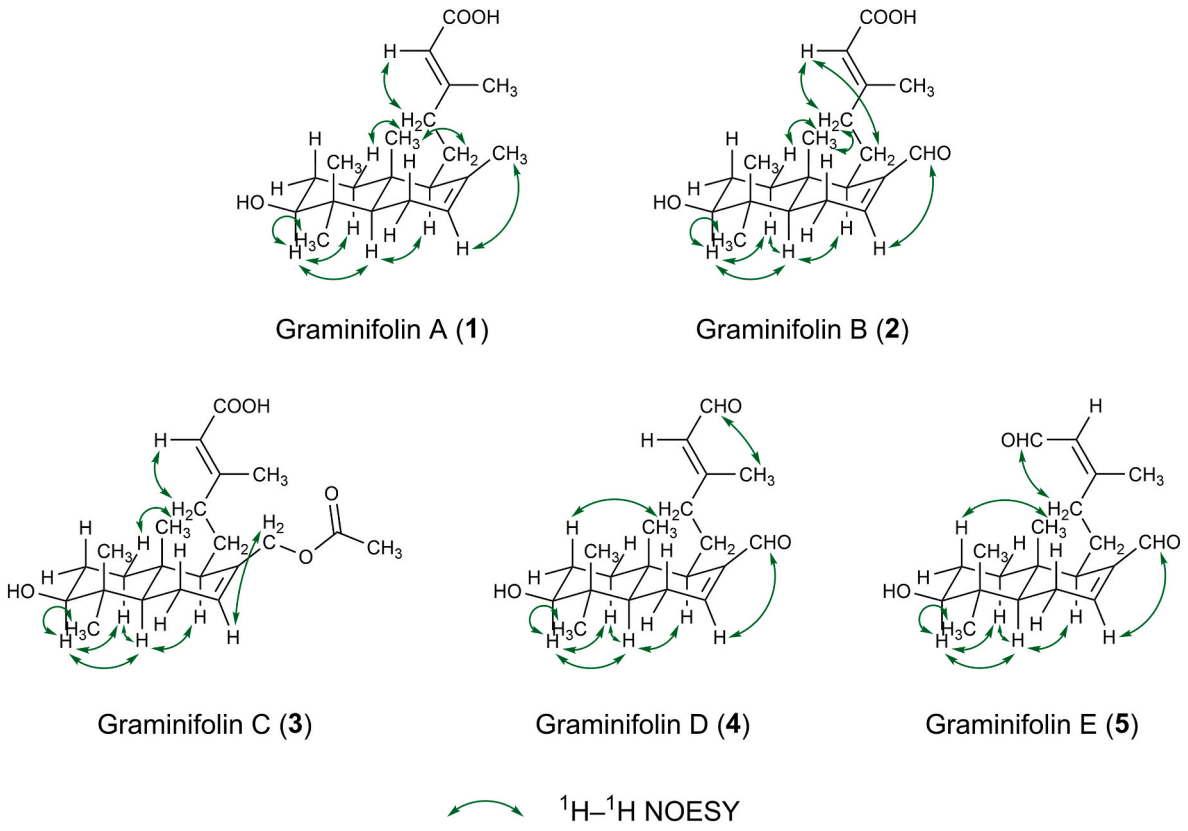

Fig. 5. Key ^{1}H–^{1}H NOESY correlations (green) of graminifolins A–E (**1**–**5**). (For interpretation of the references to color in this figure legend, the reader is referred to the Web version of this article.)

protons (H_3-16) was weakly correlated with C-15 in the HMBC spectrum, revealing the presence of a carboxylic moiety (Fig. 4).

After determining the planar structure, the relative configuration of compound **1** was elucidated by diagnostic spin-spin coupling constants and ^{1}H–^{1}H NOESY correlations (Fig. 5). The large coupling constant between H_2-2_{ax} and H-3 ($^{3}J_{H\text{-}2ax,H\text{-}3} = 10.8$ Hz) confirmed that H-3 occupied an axial position, randomly defined as α-oriented, indicating that 3-OH was β-configured. Starting from the α-oriented H-3 proton, according to the NOESY cross-peaks between H-3/H_2-1a, H-3/H-5, H-3/H_3-18, H-5/H_2-1a, H-5/H-9, H_2-1a, H-3, H-5, H-9, and H_3-18 were assigned as α. A *trans* A/B ring fusion was evident from the lack of correlation H_3-20/H-5, which was corroborated by NOE enhancements between H_3-20/H_2-1a. NOESY spectrum featured cross-peaks between H-14/H_2-12a and H-14/H_2-12b, although no correlation was observed between H-14/H_3-16, which is consistent with a double bond with *E* configuration. Compound **1** was synthesized via alkaline hydrolysis of the methyl ester of sempervirenic acid, the 3-*O*-acetyl derivative of **1**, isolated from *Solidago sempervirens* L. (Purushothaman et al., 1983) and later from *S. canadensis* (Li et al., 2014). Moreover, the methyl ester of its 13-*Z* isomer was also obtained from *Leysera gnaphaloides* (L.) Thunb. after reacting with diazomethane (Tsichritzis and Jakupovic, 1991). Thus, it has been shown that compound **1**, trivially named graminifolin A, and previously only described as a synthetic product, is also produced biosynthetically in nature.

Graminifolin B (**2**) (Fig. 3) was obtained as a colorless oil with a specific optical rotation of $[\alpha]_D^{25}$ +22.8 (*c* 1.6, $CHCl_3$). Its molecular formula was revealed to be $C_{20}H_{30}O_4$ determined from the ^{13}C NMR and positive- and negative-ion mode HESI-HRMS spectra at *m/z* 357.2035 $[M+Na]^+$ (calculated for $C_{20}H_{30}O_4Na^+$, *m/z* 357.2036 $[M+Na]^+$, error: −0.5 ppm) and *m/z* 333.2072 $[M-H]^-$ (calculated for $C_{20}H_{29}O_4^-$, *m/z* 333.2071 $[M-H]^-$, error: 0.1 ppm), demanding 6 DBEs. The ^{1}H and ^{13}C NMR spectroscopic data (Tables 1 and 2) demonstrated that compound **2** shared a similar structure to compound **1** with the only difference of the occurrence of a formyl group at C-17 (δ_H 9.37 (1H, s), δ_C 194.9) in **2** replacing the methyl group in **1**. This assumption was corroborated by the key HMBC correlations from H-17 to C-7, C-8, and C-9 (Fig. 4), the NOESY correlation between H-7/H-17, the chemical shift difference of H-7 (δ_H 6.82 in **2** compared to δ_H 5.42 in **1**, Δ = +1.40 ppm), C-7 (δ_C 153.1 in **2** compared to δ_C 123.6 in **1**, Δ = +29.6 ppm), and C-8 (δ_C 144.0 in **2** compared to δ_C 135.8 in **1**, Δ = +8.2 ppm) compared to **1** due to the electron-withdrawing effect of formyl group. The MS/MS fragmentation pattern of the precursor ion at *m/z* 333.2072 $[M-H]^-$ to give fragment ions at *m/z* 271.2067 $[M-H-CO_2-H_2O]^-$, 289.2171 $[M-H-CO_2]^-$, the bathochromic shift of its UV absorption maximum (from 209 nm in **1** to 225 nm in **2**, Δ = +16 nm) compared to **1**, the broad IR absorption band at 3401 cm^{-1} (O–H stretch) and intense, sharp bands at 1685 cm^{-1} (α,β-unsaturated C=O stretch) and 1633 cm^{-1} (C=C stretch) agree the proposed structure. The relative configuration of **2** was deduced to be the same as that of **1** by comparing their NOE interactions (Fig. 5) and coupling constants. Compound **2** was, therefore, determined to be a previously undescribed labdane diterpene, trivially named graminifolin B.

Graminifolin C (**3**) (Fig. 3) was obtained as a colorless oil with an optical rotation of $[\alpha]_D^{25}$ +2.1 (*c* 2.7, $CHCl_3$). It gave a molecular formula of $C_{22}H_{34}O_5$ based on the ^{13}C NMR data and the positive-ion HESI-HRMS peak at *m/z* 401.2298 $[M+Na]^+$ (calculated for $C_{22}H_{34}O_5Na^+$, *m/z* 401.2298 $[M+Na]^+$, error: −0.1 ppm) and the negative-ion HESI-HRMS peak at *m/z* 377.2326 $[M-H]^-$ (calculated for $C_{22}H_{33}O_5^-$, *m/z* 377.2334 $[M-H]^-$, error: −2.1 ppm), indicating 6 DBEs. The ^{1}H and ^{13}C NMR spectroscopic data (Tables 1 and 2) showed a similar structural pattern as that of compound **1** except for the diastereotopic methylene protons at δ_H 4.51 (1H, d (12.2), H_2-17a), 4.45 (1H, d (12.2), H_2-17b) at C-17 (δ_C 67.6) as well as an additional methyl resonance at δ_H 2.04 (3H, s, H_3-2′), δ_C 21.2 (C-2′) and a carbonyl carbon signal at δ_C 171.0 (C-1′). These results implied the presence of an acetoxy group attached to the labdane skeleton

at C-17, supported by the characteristic HMBC correlations from H_2-17 to C-1′, C-7, C-8, C-9 and from H_3-2′ to C-1′ (Fig. 4), and by NOESY correlations observed between H-7/H_2-17a and H-7/H_2-17b (Fig. 5). It was further verified by the MS/MS fragmentation pattern of the precursor ion at *m/z* 401.2300 $[M+Na]^+$ to yield fragment ions at *m/z* 83.0103 ($C_2H_4O_2Na^+$), 341.2089 $[M+Na–C_2H_4O_2]^+$ (loss of acetic acid) and the precursor ion at *m/z* 377.2326 $[M-H]^-$ to give fragment ions at *m/z* 59.0139 ($C_2H_3O_2^-$), 273.2224 $[M-H-C_2H_4O_2-CO_2]^-$ (loss of acetic acid and carbon dioxide), 291.2330 $[M-H-C_2H_2O-CO_2]^-$ (loss of ketene and carbon dioxide), 317.2122 $[M-H-C_2H_4O_2]^-$ (loss of acetic acid), and 335.2228 $[M-H-C_2H_2O]^-$ (loss of ketene). The proposed structure agree with the losses of carbon dioxide and the broad IR absorption band at 3407 cm^{-1} (O–H stretch) and intense, sharp bands at 1735 cm^{-1} (C═O stretch, CH_3CO–), 1691 cm^{-1} (α,β-unsaturated C═O stretch, COOH), 1641 cm^{-1} (C═C stretch), and 1235 cm^{-1} (C–O stretch, CH_3CO–). The relative configuration of **3** was elucidated to be the same as that of **1** by comparing their NOE enhancements (Fig. 5) and coupling constants. Thus, compound **3** has been identified as a previously unreported labdane diterpene, trivially named graminifolin C.

Graminifolin D (**4**) and graminifolin E (**5**) (Fig. 3) were isolated as an inseparable mixture (11:9 ratio) of (*E*)-(*Z*) isomers obtained as a yellow oil with an optical rotation of $[\alpha]_D^{25}$ −6.5 (*c* 0.3, $CHCl_3$). Both compounds shared the molecular formula $C_{20}H_{30}O_3$ as determined from ^{13}C NMR data and positive-ion mode HESI-HRMS spectrum at *m/z* 341.2087 $[M+Na]^+$ (calculated for $C_{20}H_{30}O_3Na^+$, *m/z* 341.2087 $[M+Na]^+$, error: −0.1 ppm), requiring 6 DBEs. The ^1H and ^{13}C NMR spectroscopic data (Tables 1 and 2) exhibited similarity with those of **2** except for the presence of a formyl group at C-15 (δ_H 9.98 (1H, d, $J = 8.1$ Hz, H-15), δ_C 191.7 for **4**, (δ_H 10.03 (1H, d, $J = 8.3$ Hz, H-15), δ_C 191.8 for **5**) replacing the carboxylic group in **2** as supported by a COSY correlation between H-14/H-15, HMBC correlations from H-15 to C-13, C-14 (Fig. 4), and the bathochromic shift of its UV absorption maximum (from 225 nm in **2** to 232 nm in **4**+**5**, $\Delta = +7$ nm) compared to **2**. Additionally, 1D and 2D NMR data revealed compound **4** to be a diastereomer of **5**, particularly (*E*)-(*Z*) isomers. The different ^1H and ^{13}C NMR chemical shifts of H_2-12a (δ_H 2.80 in **4**, δ_H 3.05 in **5**), H_2-12b (δ_H 2.14 in **4**, δ_H 2.63 in **5**), H-15 (δ_H 9.98 in **4**, δ_H 10.03 in **5**), H_3-16 (δ_H 2.20 in **4**, δ_H 2.02 in **5**) as well as C-11 (δ_C 25.1 in **4**, δ_C 27.0 in **5**), C-12 (δ_C 42.7 in **4**, δ_C 35.0 in **5**), and C-16 (δ_C 17.7 in **4**, δ_C 25.1 in **5**) suggested that **4** and **5** differ in the configuration of the double bond $\Delta^{13,14}$. This was confirmed by the diagnostic NOESY correlations between H-14/H_2-12a and H-14/H_2-12b for compound **4** (Fig. 5) consistent with an *E*-double-bond-geometry. However, for compound **5** NOESY spectrum featured cross-peaks between H-14/H_3-16 (Fig. 5), which permitted the assignment of its double bond configuration as *Z*. The broad IR absorption band at 3420 cm^{-1} (O–H stretch) and intense, sharp bands at 1683, 1673 cm^{-1} (α,β-unsaturated C═O stretch), and 1633 cm^{-1} (C═C stretch) agree with the proposed structure. Consequently, compounds **4** and **5** have been established as previously undescribed labdane diterpenes, trivially named graminifolin D and E, respectively. Labdane diterpenes featuring a C-13–C-14 double bond typically adopt the *E* configuration (Urones et al., 1990, 1994; Barrero et al., 2006; Barbosa et al., 2019; Zhang et al., 2020, 2023; Xu et al., 2025); however, some examples for *Z* configuration have also been reported (Bohlmann et al., 1982; Meckes et al., 2002; Simpson et al., 2012). As plants generally produce only a single geometric isomer (either *E* or *Z*), therefore, graminifolin E (**5**) is presumed to be an isolation artifact.

The absolute configurations of compounds **1**–**5** were not ascertained. However, chemotaxonomic evidence indicated that all labdane diterpenes previously isolated from *Solidago* species such as 3β-acetoxycopalic acid (Li et al., 2014), deoxysolidagenone (Wangensteen et al., 2012), presolidagenone (Móricz et al., 2020), pumiloxide (Vila et al., 2002), sempervirenic acid (Li et al., 2014), solicanolide (Bradette-Hébert et al., 2008), solidagenone (Móricz et al., 2020; Bortoleti et al., 2022; Wangensteen et al., 2012), solidagol (Li et al., 2014), and related compounds (Bohlmann et al., 1980; Hirschmann, 1988; Lu et al., 1995; Wangensteen et al., 2012), belong to the *normal*-labdane series. Thus, by analogy, compounds **1**–**5** could be assigned to the *normal*-labdane series.

2.2. Compound characterization

2.2.1. Graminifolin A (1)

Yellow oil; $[\alpha]_D^{25}$ +8.9 (*c* 0.29, MeOH); UV (EtOH) λ_{max} (log ε) 209 nm (4.03); IR (ATR) ν_{max} 3388, 2958, 2930, 2870, 2854, 1692, 1645, 1458, 1443, 1415, 1384, 1366, 1126, 1092, 1054, 1033, 1021, 1006 cm^{-1}; ^1H (400 MHz, CD_3OD) and ^{13}C (101 MHz, CD_3OD) NMR spectroscopic data, see Tables 1 and 2; HESI-HRMS *m/z* 319.2278 $[M-H]^-$ (calculated for $C_{20}H_{31}O_3^-$, *m/z* 319.2279 $[M-H]^-$, error: −0.2 ppm).

2.2.2. Graminifolin B (2)

Colorless oil; $[\alpha]_D^{25}$ +22.8 (*c* 1.6, $CHCl_3$); UV (EtOH) λ_{max} (log ε) 225 nm (4.10), 335 nm (2.13); IR (ATR) ν_{max} 3401, 3019, 2968, 2935, 2856, 1685, 1633, 1442, 1421, 1388, 1370, 1252, 1232, 1215, 1160, 1088, 1044 cm^{-1}; ^1H (400 MHz, $CDCl_3$) and ^{13}C (101 MHz, $CDCl_3$) NMR spectroscopic data, see Tables 1 and 2; HESI-HRMS *m/z* 357.2035 $[M+Na]^+$ (calculated for $C_{20}H_{30}O_4Na^+$, *m/z* 357.2036 $[M+Na]^+$, error: −0.5 ppm), *m/z* 333.2072 $[M-H]^-$ (calculated for $C_{20}H_{29}O_4^-$, *m/z* 333.2071 $[M-H]^-$, error: 0.1 ppm).

2.2.3. Graminifolin C (3)

Colorless oil; $[\alpha]_D^{25}$ +2.1 (*c* 2.7, $CHCl_3$); UV (EtOH) λ_{max} (log ε) 214 nm (4.05); IR (ATR) ν_{max} 3407, 2966, 2932, 2853, 1735, 1719, 1691, 1641, 1442, 1384, 1367, 1235, 1157, 1092, 1049, 1021 cm^{-1}; ^1H (400 MHz, $CDCl_3$) and ^{13}C (101 MHz, $CDCl_3$) NMR spectroscopic data, see Tables 1 and 2; HESI-HRMS *m/z* 401.2298 $[M+Na]^+$ (calculated for $C_{22}H_{34}O_5Na^+$, *m/z* 401.2298 $[M+Na]^+$, error: −0.1 ppm), *m/z* 377.2326 $[M-H]^-$ (calculated for $C_{22}H_{33}O_5^-$, *m/z* 377.2334 $[M-H]^-$, error: −2.1 ppm).

2.2.4. Graminifolin D (4) and graminifolin E (5) (11:9 mixture)

Yellow oil; $[\alpha]_D^{25}$ −6.5 (*c* 0.3, $CHCl_3$); UV (EtOH) λ_{max} (log ε) 206 nm (3.79), 232 nm (3.97); IR (ATR) ν_{max} 3420, 2963, 2934, 2871, 2722, 1707, 1683, 1673, 1633, 1460, 1386, 1232, 1187, 1161, 1128, 1090, 1044 cm^{-1}; ^1H (400 MHz, $CDCl_3$) and ^{13}C (101 MHz, $CDCl_3$) NMR spectroscopic data, see Tables 1 and 2; HESI-HRMS *m/z* 341.2087 $[M+Na]^+$ (calculated for $C_{20}H_{30}O_3Na^+$, *m/z* 341.2087 $[M+Na]^+$, error: −0.1 ppm).

2.3. Microdilution assays

The antibacterial activity of the isolates (compounds **1**–**3** and a mixture of compounds **4** and **5**) was assessed based on their MIC and MBC values (Table 3) against various bacterial strains and their MIC values against fungal strains. Beyond the ubiquitous soil bacterium *B. subtilis*, the Gram-positive bacterial strains included the bean pathogen *C. flaccumfaciens* pv. *flaccumfaciens*, and the tomato pathogen *C. michiganensis* (formerly known as *C. michiganensis* subsp. *michiganensis*). Their common symptom in the infected plants is the wilting leaf, with the latter also contributing to stem and fruit canker and leaf spots' formation (Agrios, 2024). To test the isolated compounds against Gram-negative bacteria, the tobacco pathogen *P. syringae* pv. *tabaci*, and tomato and *Arabidopsis thaliana* (L.) Heynh. pathogen *P. syringae* pv. *tomato* were utilized, which cause lesions with chlorotic halos on leaves and also lead to specked fruit in the case of tomato (Agrios, 2024). *F. graminearum* fungus is a major causal agent of head blight and ear rot in cereal crops such as wheat, barley, and maize. Due to its mycotoxin production, it can pose serious health risks (Dweba et al., 2017). The common root rot, seedling blight, and foliar spot blotch of plants from the *Poaceae* Barnhart family (*e.g.*, barley and wheat) can be caused by the fungus *B. sorokiniana*, especially in warm and humid environments (Kumar et al., 2002). These plant pathogens lead to substantial economic losses in their host plant production worldwide via significant

Table 3
The minimal inhibitory concentration (MIC) and minimal bactericidal concentration (MBC) values of isolated compounds (**1**–**3** and **4**+**5**) and positive controls gentamicin (Gent) and benomyl (Ben), respectively, against the *Bacillus subtilis* (*Bs*), *Curtobacterium flaccumfaciens* pv. *flaccumfaciens* (*Cff*), *Clavibacter michiganensis* (*Cm*), *Pseudomonas syringae* pv. *tabaci* (*Pstab*), and *Pseudomonas syringae* pv. *tomato* DC3000 lux (*Pstom*) bacterial strains, and *Bipolaris sorokiniana* (*Bip*) and *Fusarium graminearum* (*Fg*) fungal strains in μg/mL.

	Bs		*Cff*		*Cm*		*Pstab*		*Pstom*		*Bip*	*Fg*
	MIC	MBC	MIC	MBC	MIC	MBC	MIC	MBC	MIC	MBC	MIC	MIC
1	67	133	267	267	67	267	>533	>533	>533	>533	>533[a]	>533
2	533	>533	533	533	267	267	>533	>533	>533	>533	>533	>533
3	133	267	533	533	267	533	>533	>533	>533	>533	>533	>533
4+**5**	133	267	>533	>533	267	267	>533	>533	>533	>533	>533	>533
Gent	0.8	1.7	0.8	0.8	1.7	1.7	0.8	0.8	0.4	0.8		
Ben											1042	521

[a] 61.5% mycelium growth inhibition at the highest concentration (533 μg/mL).

yield losses and quality reduction, highlighting the importance of effective plant protection strategies.

All isolates were active against the studied Gram-positive bacterial strains, with MIC values ranging from 67 to 533 μg/mL and MBC values between 133 and 533 μg/mL, except for **4**+**5**, which did not inhibit *C. flaccumfaciens* pv. *flaccumfaciens*, and compound **2**, which did not reach the MBC against *B. subtilis* at the concentrations tested. The strongest antibacterial effect was observed for **1** against *B. subtilis* and *C. michiganensis*, with MIC values 80 and 40 times higher, respectively, than those of the positive control, gentamicin. None of the isolates inhibited the bacterial growth of the studied Gram-negative strains and only compound **1** displayed antifungal activity against *B. sorokiniana* with 61.5% mycelium growth inhibition at the highest concentration (533 μg/mL). In terms of structure-activity relationship, the oxidation at C-17 may diminish antimicrobial activity. However, this hypothesis requires further investigation to be confirmed.

The results are consistent with literature data on the antimicrobial activity of goldenrod diterpenes. Labdane (Móricz et al., 2020), clerodane (Starks et al., 2010; Baglyas et al., 2022; Móricz et al., 2021; Bozsó et al., 2024), and abietane (Baglyas et al., 2023) goldenrod diterpenes exhibited inhibitory activity similarly against Gram-positive bacterial and fungal (no data regarding labdane ones) species. Furthermore, MIC values of the isolates (**1**–**3**, **4**+**5**) were comparable to or higher than those reported for clerodane (Starks et al., 2010; Baglyas et al., 2022; Bozsó et al., 2024) and abietane (Baglyas et al., 2023) diterpenes.

2.4. Labdane diterpenes and their bioactivities

Labdane diterpenes and their reported bioactivities are introduced hereby. Labdane-type diterpenes, comprising over 7,000 natural products, are widely distributed specialized metabolites found in plants, fungi, insects, and marine organisms (Chinou, 2005; Acquaviva et al., 2022). These compounds were reported as constituents of goldenrod species, including *S. canadensis* (Bohlmann et al., 1980; Bragdette-Hébert et al., 2008; Wangensteen et al., 2012; Li et al., 2014; Móricz et al., 2020), *Solidago chilensis* Meyen (Hirschmann et al., 1988; Vila et al., 2002), and *S. rugosa* (Lu et al., 1995). Some of them, such as solidagenone and presolidagenone, displayed antibacterial activity (Móricz et al., 2020), while solicanolide exhibited cytotoxic effect (Bradette-Hébert et al., 2008). A wide-range bioactivity has been described for labdane diterpenes (Singh et al., 1999; Demetzos and Dimas, 2001), including antibacterial (Corlay et al., 2015; Heo et al., 2024), antifungal (Chakrabartty et al., 2021; Echeverría et al., 2019), cytotoxic (Heo et al., 2024; Voon et al., 2022), anti-inflammatory (Tran et al., 2017; Yin et al., 2019), insecticidal (Wang et al., 2024; Arya et al., 2024), and glucosidase (Yin et al., 2019) and acetylcholinesterase inhibitory (Hung et al., 2011) activities.

3. Conclusions

In summary, flash column chromatographic fractionation interlaced with TLC hyphenations enabled the bioassay-guided isolation of five previously undescribed labdane diterpenes, graminifolins A–E (**1**–**5**). Their structures were elucidated using NMR spectroscopy, FIA–HRMS (/MS), polarimetry, and UV and ATR–FTIR spectroscopy. This is the first report to describe diterpenes in *E. graminifolia*, which exhibited moderate antibacterial activity against three Gram-positive phytopathogenic bacteria. Furthermore, the most potent compound, graminifolin A (**1**), also moderately inhibited the growth of the crop pathogenic fungus *B. sorokiniana*. To the best of our knowledge, antimicrobial goldenrod labdane diterpenes are first published here along with their MIC values, which are consistent with previously reported data on goldenrod diterpenes. These findings suggest the potential application of graminifolins A–E to mitigate the ecological impact of synthetic pesticides, while also serving as a starting point for the development of more potent plant-derived pesticide candidates for plant protection.

4. Experimental

4.1. Materials

Isopropyl acetate, gentamicin, benomyl, and *p*-anisaldehyde were from Sigma-Aldrich (Burlington, MA, USA). Other solvents of analytical grade (methyl ethyl ketone, toluene, ethanol, methanol, chloroform, *n*-hexane, acetone) used for extraction, TLC, flash column chromatography, UV spectroscopy, polarimetry and gradient-grade methanol used for TLC–MS were purchased from Molar Chemicals (Halásztelek, Hungary) or Reanal (Budapest, Hungary). Methanol (LC-MS grade) was acquired from VWR (Radnor, PE, USA). Vanillin was obtained from Reanal and acetic acid from Lach-Ner (Neratovice, Czech Republic). Concentrated sulfuric acid (96%) was supplied by Carlo Erba (Milan, Italy). 3-(4,5-Dimethylthiazol-2-yl)-2,5-diphenyltetrazolium bromide (MTT) was purchased from Carl Roth (Karlsruhe, Germany). The Gram-positive soil bacterium *Bacillus subtilis* (strain F1276) was a gift from József Farkas (Central Food Research Institute, Budapest, Hungary). *Curtobacterium flaccumfaciens* pv. *flaccumfaciens* (NCAIM B.01609), *Pseudomonas syringae* pv. *tabaci* H10 (NCAIM B.01601), and *Fusarium graminearum* Schwabe (NCAIM F.00730) were purchased from the National Collection of Agricultural and Industrial Microorganisms (NCAIM, Budapest, Hungary). *Clavibacter michiganensis* strain was isolated from tomato in 1978 (49/1, Sándor Süle, Plant Protection Institute, HUN-REN Centre for Agricultural Research, Budapest, Hungary), and *Bipolaris sorokiniana* (Sacc.) Shoemaker H-299 (NCBI GenBank accession No. MH697869) was collected from barley in Hungary. *Pseudomonas syringae* pv. *tomato* DC3000 Lux was a kind gift from Julia Vorholt (ETH Zurich, Switzerland). The Ultrapure water was prepared by the Millipore Direct-Q 3 UV Water Purification System (Merck, Darmstadt, Germany).

4.2. Sample origin and preparation

Euthamia graminifolia flowers were collected in Hungary in the Bükk Mountains at Eger Almár (47°57′ N, 20°21′ E; 325 m a.s.l.) on August 30,

2019. Voucher plant specimens were deposited at the Herbarium of the Hungarian Natural History Museum, Budapest, Hungary, under the accession numbers HNHM-TRA00035003 and HNHM-TRA00035004. The fresh flowers were dried at room temperature and ground with a coffee grinder (Sencor SCG, 2050; Říčany, Czech Republic). The pulverized sample (100 mg) was extracted with methyl ethyl ketone (1 mL) by maceration and the filtered crude extract was used for TLC. For the isolation process, 60 g of dried flowers were macerated with methyl ethyl ketone three times (3 × 500 mL, 3 days each). The extracts were filtered (Whatman No. 2 filter paper, Sigma), merged, and dried *in vacuo* by a rotary evaporator (Rotavapor R-134, Büchi, Flawil, Switzerland) to provide 11 g of dried material.

4.3. TLC and TLC–direct bioautography

Thin-layer chromatographic analyses were carried out with TLC silica gel 60 F_{254} layers (Merck). The chromatograms were developed with the mobile phase isopropyl acetate – toluene – ethanol, 11:9:1 (*V/V*) in a twin-trough chamber (CAMAG, Muttenz, Switzerland) up to 75 mm from the lower plate edge. Samples were applied by a 10-μL microsyringe (Hamilton, Bonaduz, Switzerland) as the 5-mm bands with 6-10-mm track distance and 8-mm distance from the lower edge. After development, plates were dried by a cold air stream of a hair dryer and documented under a UV lamp (CAMAG) at 254 nm and 366 nm, or visible light after derivatization with vanillin–sulfuric acid reagent (400 mg of vanillin, 100 mL of ethanol, and 2 mL of concentrated sulfuric acid (96%); heating at 110 °C for 5 min, Advanced Hot Plate, VWR), or anisaldehyde reagent (500 μL of *p*-anisaldehyde, 10 mL of acetic acid, 100 mL of methanol, and 5 mL of concentrated sulfuric acid (96%); heating at 110 °C for 5 min, Advanced Hot Plate), or *B. subtilis* bioassay.

The TLC–*B. subtilis* assay was performed as described (Móricz et al., 2015). Briefly, the dried chromatoplates were dipped into the bacterial cell suspension (OD_{600} = 1.2, 5 × 10^8 CFU/mL) and after a 2-h incubation (at 37 °C and 100% humidity), immersed into a vital dye solution (MTT, 1 mg/mL in water) and incubated for an additional 15 min. The bioautograms were documented with a digital camera (Cybershot DSC-HX60, Sony, Neu-Isenberg, Germany) under visible light. Antibacterial compounds appeared as bright zones against a purple background. The background under the chromatographic alpha front was used as a negative control and the fatty acid linoleic acid as a positive control.

4.4. Compound isolation by flash column chromatography

Fractionation and isolation of bioactive compounds of *E. graminifolia* flowers were performed by preparative flash column chromatography (CombiFlash NextGen 300, Teledyne Isco, Lincoln, NE, USA) using silica gel columns (RediSep Rf Gold, 20–40 μm, 12, 24, and 40 g, Teledyne Isco) and a C_{18} column (RediSep Rf Gold, 20–40 μm, 30 g, Teledyne Isco).

The dried crude extract (11.0 g) was re-suspended with 3 mL of chloroform and subjected to preparative flash chromatography using a silica gel column (RediSep Rf Gold, 20–40 μm, 40 g) and a gradient system of *n*-hexane and acetone (0–0.5 min, 0%; 0.5–10 min, 0–30%; 10–17 min, 30–50%; 17–18 min, 50–100%; 18–23 min, 100% acetone) with a 40 mL/min eluent flow rate yielding three pooled fractions: 21–26 (**I**, t_R = 8.1–10.0 min, 136.9 mg), 27–34 (**II**, t_R = 10.0–12.8 min, 356.2 mg), and 35–41 (**III**, t_R = 12.8–16.1 min, 724.2 mg). All combined fractions were dried, re-suspended in chloroform, and further fractionated on a C_{18} column (RediSep Rf Gold, 20–40 μm, 30 g) using a gradient system of water with 0.1% formic acid and methanol (0–1 min, 50%; 1–16 min, 50–90%; 16–18 min, 90–100%; 18–25 min, 100% methanol) with 20 mL/min eluent flow rate giving active fractions **I**/29–30 (t_R = 13.9–15.0 min, 16.9 mg), **I**/38–39 (t_R = 17.9–19.4 min, 16.1 mg), **II**/23–25 (t_R = 10.8–12.7 min, 128.5 mg), **II**/28–29 (t_R = 13.5–14.9 min, 59.1 mg), **II**/37 (t_R = 18.5–19.0 min, 20.8 mg), and **III**/34–35 (t_R = 14.1–16.0 min, 53.6 mg). Fractions **I**/38–39 and **II**/37 were merged, re-suspended in chloroform and further purified on a silica gel column (Redisep Rf Gold, 20–40 μm, 12 g) using a gradient system of *n*-hexane and acetone (0–1 min, 0–25%; 1–11 min, 25% acetone) with 15 mL/min eluent flow rate to provide compound **1** (fraction 12–15, t_R = 5.8–9.3 min, 8.2 mg). Fraction **II**/23–25 was re-suspended in chloroform and further purified on a silica gel column (Redisep Rf Gold, 20–40 μm, 24 g) using a gradient system of *n*-hexane and acetone (0–0.5 min, 0%; 0.5–1 min, 0–20%; 1–19 min, 20%; 19–20.5 min, 20–73%; 20.5–25.5 min, 73%; 25.5–26 min, 73–100%; 26–27 min, 100% acetone) with 20 mL/min eluent flow rate to afford compounds **4**+**5** (fraction 19–20, t_R = 11.3–13.2 min, 8.8 mg) and **2** (fraction 34, t_R = 22.1–22.3 min, 36.8 mg). Fractions **I**/29–30, **II**/28–29, and **III**/34–35 were merged and re-suspended in chloroform and further purified on a silica gel column (Redisep Rf Gold, 20–40 μm, 12 g) using a gradient system of *n*-hexane and acetone (0–1 min, 0–20%; 1–14 min, 20% acetone) with 20 mL/min eluent flow rate to yield compound **3** (fraction 23–27, t_R = 10.2–11.9 min, 66 mg).

4.5. Spectroscopic and spectrometric characterization of the compounds

For TLC–MS, the binary HPLC pump (LC-20AB, Shimadzu, Kyoto, Japan) guided the methanol at a flow rate of 0.2 mL/min through the oval elution head (4 mm × 2 mm) of the TLC-MS Interface 2 (CAMAG) to a single quadrupole electrospray ionization mass spectrometer (LCMS-2020, Shimadzu). The instrument control and data acquisition were performed using the LabSolutions 5.42v software (Shimadzu). HRMS (/MS) spectra of isolated compounds were recorded by flow injection analysis (FIA) using the combination of a UHPLC (Vanquish Flex VF-P10, Dionex Softron, Germering, Germany) and a hybrid quadrupole-orbitrap mass spectrometer with HESI-II probe (Orbitrap Exploris 120, Thermo Fisher Scientific, Bremen, Germany). All NMR spectra were acquired either on a Varian Mercury Plus 400 (^{1}H: 400.0 MHz, ^{13}C: 100.6 MHz; 9.4 T) spectrometer equipped with a Varian 400 Automation Triple Resonance Broadband Pulsed Field Gradient (ATB PFG) probe head or a Bruker AVANCE III 500 (^{1}H: 500.1 MHz, ^{13}C: 125.8 MHz; 11.7 T) spectrometer equipped with a 5 mm triple-resonance, z-gradient cryoprobe (CP TCI 500S2 H–C/N-D-05 Z) (Bruker Corporation, Billerica, MA, USA) at 298 or 296 K, respectively. One-dimensional (1D) ^{1}H, ^{13}C, and ^{13}C DEPTQ as well as two-dimensional (2D) homonuclear ^{1}H–^{1}H COSY and ^{1}H–^{1}H NOESY, and heteronuclear ^{1}H–^{13}C edHSQC and ^{1}H–^{13}C HMBC (optimized for $^nJ_{C–H}$ = 8 Hz) spectra were acquired in methanol-d_4 (≥99.8 atom% D, Merck) or chloroform-*d* (99.8 atom% D, Merck), and all pulse sequences were taken from the spectrometer software libraries (VnmrJ 3.1 or TopSpin 3.5). Optical rotations were measured at 25 °C on a PerkinElmer 341 LC polarimeter (Waltham, MA, USA) in methanol (compound **1**) or chloroform (compounds **2**–**5**) at 589.3 nm (D-line of sodium). UV absorption spectra were recorded at room temperature in ethanol using a PerkinElmer Lambda 35 spectrophotometer. ATR-FTIR spectra were acquired on a PerkinElmer Spectrum 400 FT-IR/FT-NIR spectrometer equipped with a diamond/ZnSe ATR crystal and a MIR TGS detector. A more detailed description of the methods can be found in the Supporting Information (M1–M4).

4.6. Evaluation of the antibacterial, bactericidal, and antifungal activity of isolated compounds

Determination of the minimal inhibitory concentration (MIC) of the isolates against the *B. subtilis*, *C. flaccumfaciens* pv. *flaccumfaciens*, and *C. michiganensis* bacterial growth was performed using non-treated, flat-bottom 96-well microplates (VWR, cat #734–2781). The experimental procedures of these assays were based on the methods previously described (Baglyas et al., 2023; Cselőtey et al., 2024) with slight modifications. The microdilution assay with *P. syringae* pv. *tabaci* and *P. syringae* pv. *tomato* was carried out with a procedure similar to that with *B. subtilis*. Briefly, *B. subtilis* was grown in Luria-Bertani (LB) broth

(10 g/L tryptone (Reanal), 5 g/L yeast extract (Scharlau, Barcelona, Spain) and 10 g/L sodium chloride (Reanal)) at 37 °C, *P. syringae* pv. *tabaci* and *P. syringae* pv. *tomato* were grown in LB broth at 28 °C, while *C. flaccumfaciens* pv. *flaccumfaciens* and *C. michiganensis* were cultured in Nutrient Broth (NB) (11 g/L peptones, 5 g/L sodium chloride) (Biolab, Budapest, Hungary)) at 28 °C by shaking at 120 rpm. A two-fold ethanolic dilution series of 10 μL of the ethanolic solution of isolates **1** (4 mg/mL), **2** (8 mg/mL), **3** (8 mg/mL), and **4**+**5** (4 mg/mL) and 5 μL of gentamicin (positive control, 0.1 mg/mL in water) was prepared in the microplates in triplicate. Ethanol was the negative control. Ethanol was evaporated from the wells in a sterile box, and 150 μL of bacterial suspension (10^5 CFU/mL) was added to each well. The absorbance at 600 nm was measured by a spectrophotometer (Clariostar® Plus microplate reader, BMG LABTECH, Ortenberg, Germany) immediately and after 24 h (*B. subtilis*, *P. syringae* pv. *tabaci*, and *P. syringae* pv. *tomato*) or 48 h (*C. flaccumfaciens* pv. *flaccumfaciens* and *C. michiganensis*) incubation at 37 °C or 28 °C by shaking at 500 rpm with a Grant PHMP microplate shaker (Grant Instruments, Royston, United Kingdom). The experiment was repeated on two separate occasions.

The MIC values against the fungal strain *B. sorokiniana* were determined as described (Krüzselyi et al., 2021), and the method developed for *Fusarium avenaceum* (Krüzselyi et al., 2021) was adapted to *F. graminearum*. Shortly, fungi were grown for 72 h in LB at 21 °C by shaking at 120 rpm and then the mycelium was cut to small pieces with a FastPrep®-24 Classic homogenizer (MP Biomedicals, Irvine, CA, USA). Non-treated, U-bottom, 96-well microplates (Nest Scientific, Woodbridge, NJ, USA, cat #701111) were used for the microdilution assay. Benomyl (25 mg/mL in ethanol) was the positive, while ethanol was the negative control. After the evaporation of the ethanol, 70 μL of LB and then 50 μL of a mycelium suspension ($OD_{600} = 0.2$ in LB) were added to each well. The absorbance at 600 nm was measured immediately and after 72 h incubation at 21 °C.

For MBC determination, 5 μL of the sample was taken from the wells in the microplate where no bacterial growth was observed after 24 h or 48 h incubation, and was then dotted onto the surface of LB (*B. subtilis*) or NB (*C. flaccumfaciens* pv. *flaccumfaciens* and *C. michiganensis*) agar plates. The MBC was defined as the lowest concentration of the isolated compound at which no colonies formed after 24 h (*B. subtilis*) or 48 h (*C. flaccumfaciens* pv. *flaccumfaciens* and *C. michiganensis*) incubation.

CRediT authorship contribution statement

Márton Baglyas: Writing – review & editing, Writing – original draft, Investigation, Data curation. **Zoltán Bozsó:** Writing – review & editing, Investigation. **Ildikó Schwarczinger:** Writing – review & editing, Investigation. **Péter G. Ott:** Writing – review & editing, Investigation. **József Bakonyi:** Writing – review & editing, Investigation. **András Darcsi:** Investigation. **Ágnes M. Móricz:** Writing – review & editing, Writing – original draft, Supervision, Resources, Project administration, Methodology, Investigation, Funding acquisition, Data curation, Conceptualization.

Declaration of competing interest

The authors declare that they have no known competing financial interests or personal relationships that could have appeared to influence the work reported in this paper.

Acknowledgments

This work was funded by the National Research, Development and Innovation Office of Hungary (K128921 and SNN139496, Á.M.M.). The authors express their gratitude to Dóra Bogdán (Department of Organic Chemistry, Semmelweis University, Budapest, Hungary) and Tamás Gáti (Servier Research Institute of Medicinal Chemistry (SRIMC), Budapest, Hungary) for conducting NMR measurements. The authors are also grateful to Judit Nyiri (Pharmaceutical Chemistry and Technology Department, National Center for Public Health and Pharmacy, Budapest, Hungary) for her assistance in measuring optical rotations and recording ATR-FTIR and UV spectra. The authors wish to thank Péter Csontos (Institute for Soil Sciences, HUN-REN Centre for Agricultural Research, Budapest, Hungary) for the collection and identification of the plant.

Appendix B. Supplementary data

Supplementary data to this article can be found online at https://doi.org/10.1016/j.phytochem.2025.114674.

Data availability

Data will be made available on request.

References

Agrios, 2024. Plant Pathology. Elsevier. https://doi.org/10.1016/C2019-0-04179-9.
Acquaviva, R., Malfa, G.A., Loizzo, M.R., Xiao, J., Bianchi, S., Tundis, R., 2022. Advances on natural abietane, labdane and clerodane diterpenes as anti-cancer agents: sources and mechanisms of action. Molecules 27, 4791. https://doi.org/10.3390/molecules27154791.
Arya, S., Kumar, R., Karakoti, H., Mahawer, S.K., Nagarkoti, K., Prakash, O., Kumar, S., Chamoli, S., Kumar, P., Srivastava, R.M., Olievera, M.S., 2024. Pesticide and antimicrobial evaluation of three labdane-type diterpenes, and one flavonoid glycoside, isolated from rhizomes of *Hedychium coronarium* J. Koenig. Nat. Prod. Res. 1–7. https://doi.org/10.1080/14786419.2024.2413035.
Baglyas, M., Ott, P.G., Garádi, Z., Glavnik, V., Béni, S., Vovk, I., Móricz, Á.M., 2022. High-performance thin-layer chromatography – antibacterial assay first reveals bioactive clerodane diterpenes in giant goldenrod (*Solidago gigantea* Ait.). J. Chromatogr. A 1677, 463308. https://doi.org/10.1016/j.chroma.2022.463308.
Baglyas, M., Ott, P.G., Schwarczinger, I., Nagy, J.K., Darcsi, A., Bakonyi, J., Móricz, Á.M., 2023. Antimicrobial diterpenes from rough goldenrod (*Solidago rugosa* Mill.). Molecules 28, 3790. https://doi.org/10.3390/molecules28093790.
Barbosa, A.L.P., Wenzel-Storjohann, A., Barbosa, J.D., Zidorn, C., Peifer, C., Tasdemir, D., Çiçek, S.S., 2019. Antimicrobial and cytotoxic effects of the *Copaifera reticulata* oleoresin and its main diterpene acids. J. Ethnopharmacol. 233, 94–100. https://doi.org/10.1016/j.jep.2018.11.029.
Barrero, A.F., Herrador, M.M., Arteaga, P., Rosas-Romero, A., Arteaga, J.F., 2006. Antioxidant activity of diterpenes and polyphenols from *Ophryosporus heptanthus*. J. Agric. Food Chem. 54, 2537–2542. https://doi.org/10.1021/jf0527549.
Bohlmann, F., Bapuji, M., Jakupovic, J., King, R.M., Robinson, H., 1982. Unusual diterpenes from *Brickellia eupatoriedes*. Phytochemistry 21, 181–186. https://doi.org/10.1016/0031-9422(82)80039-3.
Bohlmann, F., Fritz, U., King, R.M., Robinson, H., 1980. Sesquiterpene and diterpene derivatives from *Solidago* species. Phytochemistry 19, 2655–2661. https://doi.org/10.1016/S0031-9422(00)83939-4.
Bortoleti, B.T. da S., Detoni, M.B., Gonçalves, M.D., Tomiotto-Pellissier, F., Silva, T.F., Concato, V.M., Rodrigues, A.C.J., Carloto, A.C., de Matos, R.L.N., Fattori, V., Arakawa, N.S., Verri Jr, W.A., Costa, I.N., Conchon-Costa, I., Miranda-Sapla, M.M., Wowk, P.F., Pavanelli, W.R., 2022. Solidagenone in vivo leishmanicidal activity acting in tissue repair response, and immunomodulatory capacity in *Leishmania amazonensis*. Chem. Biol. Interact. 361, 109969. https://doi.org/10.1016/j.cbi.2022.109969.
Bozsó, Z., Lapat, V., Ott, P.G., Móricz, Á.M., 2024. Disparate effects of two clerodane diterpenes of giant goldenrod (*Solidago gigantea* Ait.) on *Bacillus spizizenii*. Int. J. Mol. Sci. 25, 1531. https://doi.org/10.3390/ijms25031531.
Bradette-Hébert, M.-E., Legault, J., Lavoie, S., Pichette, A., 2008. A new labdane diterpene from the flowers of *Solidago canadensis*. Chem. Pharm. Bull. 56, 82–84. https://doi.org/10.1248/cpb.56.82.
Budzianowski, J., 1990. Two di-C-glycosylflavones from *Solidago graminifolia*. Sci. Pharm. 58, 413–416.
Butcko, V.M., Jensen, R.J., 2002. Evidence of tissue-specific allelopathic activity in *Euthamia graminifolia* and *Solidago canadensis* (Asteraceae). Am. Midl. Nat. 148, 253–262.
Chakrabartty, I., Vijayasekhar, A., Rangan, L., 2021. Therapeutic potential of labdane diterpene isolated from *Alpinia nigra*: detailed hemato-compatibility and antimicrobial studies. Nat. Prod. Res. 35, 1000–1004. https://doi.org/10.1080/14786419.2019.1610756.
Chinou, I., 2005. Labdanes of natural origin-biological activities (1981-2004). Curr. Med. Chem. 12, 1295–1317. https://doi.org/10.2174/0929867054020990.
Corlay, N., Lecsö-Bornet, M., Leborgne, E., Blanchard, F., Cachet, X., Bignon, J., Roussi, F., Butel, M.-J., Awang, K., Litaudon, M., 2015. Antibacterial labdane diterpenoids from *Vitex vestita*. J. Nat. Prod. 78, 1348–1356. https://doi.org/10.1021/acs.jnatprod.5b00206.
Cselőtey, A., Baglyas, M., Király, N., Ott, P.G., Glavnik, V., Vovk, I., Móricz, Á.M., 2024. Bioassay-guided isolation and identification of antibacterial compounds from invasive tree of heaven stem and trunk bark. Molecules 29, 5846. https://doi.org/10.3390/molecules29245846.

Demetzos, C., Dimas, K.S., 2001. Labdane-Type Diterpenes: Chemistry and Biological Activity, pp. 235–292. https://doi.org/10.1016/S1572-5995(01)80009-0.
Densmore, F., 2005. Strength of the Earth: the Classic Guide to Ojibwe Uses of Native Plants. Minnesota Historical Society, Saint Paul, MN.
Dweba, C.C., Figlan, S., Shimelis, H.A., Motaung, T.E., Sydenham, S., Mwadzingeni, L., Tsilo, T.J., 2017. Fusarium head blight of wheat: pathogenesis and control strategies. Crop Prot. 91, 114–122. https://doi.org/10.1016/j.cropro.2016.10.002.
Echeverría, J., González-Teuber, M., Urzúa, A., 2019. Antifungal activity against *Botrytis cinerea* of labdane-type diterpenoids isolated from the resinous exudate of *Haplopappus velutinus* Remy (Asteraceae). Nat. Prod. Res. 33, 2408–2412. https://doi.org/10.1080/14786419.2018.1443093.
Heo, C.-S., Kang, J.S., Yang, J.-W., Lee, M.A., Lee, H.-S., Shin, H.J., 2024. Labdane-type diterpenoids from *Streptomyces griseorubens* and their antimicrobial and cytotoxic activities. Int. J. Mol. Sci. 25, 3311. https://doi.org/10.3390/ijms25063311.
Herrera-Mayorga, V., Guerrero-Sánchez, J.A., Méndez-Álvarez, D., Paredes-Sánchez, F. A., Rodríguez-Duran, L.V., Niño-García, N., Paz-González, A.D., Rivera, G., 2022. Insecticidal activity of organic extracts of *Solidago graminifolia* and its main metabolites (quercetin and chlorogenic acid) against *Spodoptera frugiperda*: an in vitro and in silico approach. Molecules 27, 3325. https://doi.org/10.3390/molecules27103325.
Hirschmann, G., 1988. A labdan diterpene from *Solidago chilensis* roots. Planta Med. 54, 179–180. https://doi.org/10.1055/s-2006-962388.
Hung, T.M., Luan, T.C., Vinh, B.T., Cuong, T.D., Min, B.S., 2011. Labdane-type diterpenoids from *Leonurus heterophyllus* and their cholinesterase inhibitory activity. Phyther. Res. 25, 611–614. https://doi.org/10.1002/ptr.3307.
Iwu, C.D., Korsten, L., Okoh, A.I., 2020. The incidence of antibiotic resistance within and beyond the agricultural ecosystem: a concern for public health. Microbiologyopen 9, e1035. https://doi.org/10.1002/mbo3.1035.
Kalemba, D., 1992. Phenolic acids in four *Solidago* species. Pharmazie 47, 471–472.
Kalemba, D., Thiem, B., 2004. Constituents of the essential oils of four micropropagated *Solidago* species. Flavour Fragrance J. 19, 40–43. https://doi.org/10.1002/ffj.1271.
Kalemba, D., Weyerstahl, P., Marschall, H., 1994. Constituents of the essential oil of *Solidago graminifolia* (L.) Salisb. Flavour Fragrance J. 9, 269–274. https://doi.org/10.1002/ffj.2730090514.
Kruk, J., Aboul-Enein, B.H., Duchnik, E., Marchlewicz, M., 2022. Antioxidative properties of phenolic compounds and their effect on oxidative stress induced by severe physical exercise. J. Physiol. Sci. 72, 19. https://doi.org/10.1186/s12576-022-00845-1.
Krüzselyi, D., Bakonyi, J., Ott, P.G., Darcsi, A., Csontos, P., Morlock, G.E., Móricz, Á.M., 2021. Goldenrod root compounds active against crop pathogenic fungi. J. Agric. Food Chem. 69, 12686–12694. https://doi.org/10.1021/acs.jafc.1c03676.
Kumar, J., Schäfer, P., Hückelhoven, R., Langen, G., Baltruschat, H., Stein, E., Nagarajan, S., Kogel, K., 2002. *Bipolaris sorokiniana*, a cereal pathogen of global concern: cytological and molecular approaches towards better control. Mol. Plant Pathol. 3, 185–195. https://doi.org/10.1046/j.1364-3703.2002.00120.x.
Lam, J., Christensen, L.P., Färch, T., Thomasen, T., 1992. Acetylenes from the roots of *Solidago* species. Phytochemistry 31, 4159–4161. https://doi.org/10.1016/0031-9422(92)80433-F.
Li, J., Pan, L., Fletcher, J.N., Lv, W., Deng, Y., Vincent, M.A., Slack, J.P., McCluskey, T.S., Jia, Z., Cushman, M., Kinghorn, A.D., 2014. In vitro evaluation of potential bitterness-masking terpenoids from the Canada goldenrod (*Solidago canadensis*). J. Nat. Prod. 77, 1739–1743. https://doi.org/10.1021/np5001413.
Lu, T., Vargas, D., Franzblau, S.G., Fischer, N.H., 1995. Diterpenes from *Solidago rugosa*. Phytochemistry 38, 451–456. https://doi.org/10.1016/0031-9422(94)00625-4.
Mann, A., Nehra, K., Rana, J.S., Dahiya, T., 2021. Antibiotic resistance in agriculture: perspectives on upcoming strategies to overcome upsurge in resistance. Curr. Res. Microb. Sci. 2, 100030. https://doi.org/10.1016/j.crmicr.2021.100030.
Meckes, M., Calzada, F., Paz, D., Rodríguez, J., Ponce-Monter, H., 2002. Inhibitory effect of xanthomicrol and 3α-angeloyloxy-2α-hydroxy-13,14Z-dehydrocativic acid from *Brickellia paniculata* on the contractility of guinea-pig ileum. Planta Med. 68, 467–469. https://doi.org/10.1055/s-2002-32092.
Móricz, Á.M., Häbe, T.T., Böszörményi, A., Ott, P.G., Morlock, G.E., 2015. Tracking and identification of antibacterial components in the essential oil of *Tanacetum vulgare* L. by the combination of high-performance thin-layer chromatography with direct bioautography and mass spectrometry. J. Chromatogr. A 1422, 310–317. https://doi.org/10.1016/j.chroma.2015.10.010.
Móricz, Á.M., Jamshidi-Aidji, M., Krüzselyi, D., Darcsi, A., Böszörményi, A., Csontos, P., Béni, S., Ott, P.G., Morlock, G.E., 2020. Distinction and valorization of 30 root extracts of five goldenrod (*Solidago*) species. J. Chromatogr. A 1611, 460602. https://doi.org/10.1016/j.chroma.2019.460602.
Móricz, Á.M., Krüzselyi, D., Ott, P.G., Garádi, Z., Béni, S., Morlock, G.E., Bakonyi, J., 2021. Bioactive clerodane diterpenes of giant goldenrod (*Solidago gigantea* Ait.) root extract. J. Chromatogr. A 1635, 461727. https://doi.org/10.1016/j.chroma.2020.461727.
Móricz, Á.M., Ott, P.G., Häbe, T.T., Darcsi, A., Böszörményi, A., Alberti, Á., Krüzselyi, D., Csontos, P., Béni, S., Morlock, G.E., 2016. Effect-directed discovery of bioactive compounds followed by highly targeted characterization, isolation and identification, exemplarily shown for *Solidago virgaurea*. Anal. Chem. 88, 8202–8209. https://doi.org/10.1021/acs.analchem.6b02007.
Peters, R.J., 2010. Two rings in them all: the labdane-related diterpenoids. Nat. Prod. Rep. 27, 1521–1530. https://doi.org/10.1039/c0np00019a.
Price, J.S., Bever, J.D., Clay, K., 2004. Genotype, environment, and genotype by environment interactions determine quantitative resistance to leaf rust (*Coleosporium asterum*) in *Euthamia graminifolia* (Asteraceae). New Phytol. 162, 729–743. https://doi.org/10.1111/j.1469-8137.2004.01082.x.
Purushothaman, K.K., Sarada, A., Saraswathy, A., Connolly, J.D., 1983. Sempervirenic acid, a diterpene acid from *Solidago sempervirens*. Phytochemistry 22, 1042–1043. https://doi.org/10.1016/0031-9422(83)85058-4.
Schmotzer, A., 2008. A fűlevelű aranyvessző [*Solidago graminifolia* (L.) Salisb.] előfordulása Magyarországon. Flora Pannonica 6, 59–77.
Simpson, B.S., Claudie, D.J., Smith, N.M., McKinnon, R.A., Semple, S.J., 2012. Rare, seven-membered cyclic ether labdane diterpenoid from *Dodonaea polyandra*. Phytochemistry 84, 141–146. https://doi.org/10.1016/j.phytochem.2012.07.016.
Singh, M., Pal, M., Sharma, R.P., 1999. Biological activity of the labdane diterpenes. Planta Med. 65, 2–8. https://doi.org/10.1055/s-1999-13952.
Starks, C.M., Williams, R.B., Goering, M.G., O'Neil-Johnson, M., Norman, V.L., Hu, J.-F., Garo, E., Hough, G.W., Rice, S.M., Eldridge, G.R., 2010. Antibacterial clerodane diterpenes from goldenrod (*Solidago virgaurea*). Phytochemistry 71, 104–109. https://doi.org/10.1016/j.phytochem.2009.09.032.
Szymura, M., Szymura, T.H., Rajsz, A., Świerszcz, S., 2019. Is phenotypic plasticity an explanation for the invasiveness of goldenrods (*Solidago* and *Euthamia*) in Europe? Plant Species Biol. 34, 73–84. https://doi.org/10.1111/1442-1984.12236.
Thiem, B., Wesołowska, M., Skrzypczak, L., Budzianowski, J., 2001. Phenolic compounds in two *Solidago* L. species from in vitro culture. Acta Pol. Pharm. 58, 277–281.
Toiu, A., Vlase, L., Vodnar, D.C., Gheldiu, A.-M., Oniga, I., 2019. *Solidago graminifolia* L. Salisb. (Asteraceae) as a valuable source of bioactive polyphenols: HPLC profile, in vitro antioxidant and antimicrobial potential. Molecules 24, 2666. https://doi.org/10.3390/molecules24142666.
Tran, Q.T.N., Wong, W.S.F., Chai, C.L.L., 2017. Labdane diterpenoids as potential anti-inflammatory agents. Pharmacol. Res. 124, 43–63. https://doi.org/10.1016/j.phrs.2017.07.019.
Tsichritzis, F., Jakupovic, J., 1991. Diterpenes from *Leyssera gnaphaloides*. Phytochemistry 30, 211–213. https://doi.org/10.1016/0031-9422(91)84127-E.
Urones, J.G., Marcos, I.S., Basabe, P., Diez, D., Garrido, N.M., Alonso, C., Oliva, I.M., Lithgow, A.M., Moro, R.F., Sexmero, M.J., Lopez, C., 1994. Compounds with the labdane skeleton from *Halimium viscosum*. Phytochemistry 35, 713–719. https://doi.org/10.1016/S0031-9422(00)90593-4.
Urones, J.G., Marcos, I.S., Cubillo, I., Garrido, N.M., Basabe, P., 1990. Terpenoid compounds from *Parentucellia latifolia*. Phytochemistry 29, 2223–2228. https://doi.org/10.1016/0031-9422(90)83042-Y.
Vila, R., Mundina, M., Tomi, F., Furlán, R., Zacchino, S., Casanova, J., Cañigueral, S., 2002. Composition and antifungal activity of the essential oil of *Solidago chilensis*. Planta Med. 68, 164–167. https://doi.org/10.1055/s-2002-20253.
Voon, K.J., Sivasothy, Y., Sundralingam, U., Lalmahomed, A., Goh, A.P.-T., 2022. Cytotoxic labdane diterpenes, norlabdane diterpenes and bis-labdanic diterpenes from the Zingiberaceae: a systematic review. Pharmaceuticals 15, 1517. https://doi.org/10.3390/ph15121517.
Wang, Y., Lv, M., Gu, S., Hao, C., Zhou, Y., Chen, L., Xu, H., 2024. Synthesis and pesticidal activities of ester derivatives of the labdane diterpenoid andrographolide at the C-3 position containing the isoxazoline fragment and their toxicology study against *Tetranychus cinnabarinus* Boisduval. J. Agric. Food Chem. 72, 25023–25033. https://doi.org/10.1021/acs.jafc.4c07412.
Wangensteen, H., Phan, T.T., Rise, F., Halvorsen, T.G., Malterud, K.E., 2012. New labdane diterpenes from *Solidago canadensis*. Nat. Prod. Res. 26, 1348–1354. https://doi.org/10.1080/14786419.2011.565005.
Weber, E., 1998. The dynamics of plant invasions: a case study of three exotic goldenrod species (*Solidago* L.) in Europe. J. Biogeogr. 25, 147–154. https://doi.org/10.1046/j.1365-2699.1998.251119.x.
White, S.N., Boyd, N.S., Van Acker, R.C., 2016. Evaluation of aminocyclopyrachlor applied aloneand in combination with registered herbicides for crop tolerance and weed control in wild blueberry (*Vaccinium angustifolium* Ait.). Can. J. Plant Sci. 96, 11–16. https://doi.org/10.1139/cjps-2015-0214.
Xu, Q.-J., Liu, J.-C., Xu, J., Wang, X., Shang, X.-Y., Zi, J., 2025. Antimicrobial diterpenoids from *Rosmarinus officinalis*. Steroids 217, 109589. https://doi.org/10.1016/j.steroids.2025.109589.
Yin, H., Dan, W.-J., Fan, B.-Y., Guo, C., Wu, K., Li, D., Xian, K.-F., Pescitelli, G., Gao, J.-M., 2019. Anti-inflammatory and α-glucosidase inhibitory activities of labdane and norlabdane diterpenoids from the rhizomes of *Amomum villosum*. J. Nat. Prod. 82, 2963–2971. https://doi.org/10.1021/acs.jnatprod.9b00283.
Zhang, F., Ma, C., Che, Q., Zhu, T., Zhang, G., Li, D., 2023. Extending the structural diversity of labdane diterpenoids from marine-derived fungus *Talaromyces* sp. HDN151403 using heterologous expression. Mar. Drugs 21, 628. https://doi.org/10.3390/md21120628.
Zhang, X.-J., Zhong, W.-M., Liu, R.-X., Wang, Y.-M., Luo, T., Zou, Y., Qin, H.-Y., Li, X.-L., Zhang, R., Xiao, W.-L., 2020. Structurally diverse labdane diterpenoids from *Leonurus japonicus* and their anti-inflammatory properties in LPS-induced RAW264.7 Cells. J. Nat. Prod. 83, 2545–2558. https://doi.org/10.1021/acs.jnatprod.9b00597.